Nanotubes effectively deliver siRNA to intact plant cells and protect siRNA against nuclease degradation

Gozde S. Demirer[1], Huan Zhang[1], Natalie S. Goh[1], Roger Chang[1] and Markita P. Landry[1,2,3]*

[1] Department of Chemical and Biomolecular Engineering, University of California, Berkeley, CA 94720, USA.

[2] California Institute for Quantitative Biosciences, QB3, University of California, Berkeley, CA 94720, USA.

[3] Chan-Zuckerberg Biohub, San Francisco, CA 94158, USA.

*e-mail: landry@berkeley.edu

Abstract

Post-transcriptional gene silencing (PTGS) is a powerful tool to understand and control plant metabolic pathways, which is central to plant biotechnology. PTGS is commonly accomplished through delivery of small interfering RNA (siRNA) into cells. While siRNA delivery has been optimized for mammalian systems, it remains a significant challenge for plants due to the plant cell wall. Standard plant siRNA delivery methods (*Agrobacterium* and viruses) involve coding siRNA into DNA vectors, and are only tractable for certain plant species. Herein, we develop a nanotube-based platform for direct delivery of siRNA, and show high silencing efficiency in intact plant cells. We demonstrate that nanotubes successfully deliver siRNA and silence endogenous genes owing to effective intracellular delivery and nanotube-induced protection of siRNA from nuclease degradation. This study establishes that nanotubes, which are below the size exclusion limit of the plant cell wall, could enable a myriad of plant biotechnology applications that rely on RNA delivery.

Introduction

Plants are central in providing over 25% of our most clinically-relevant drugs, are at the core of our sustainability efforts, and will benefit from genetic engineering to feed our growing population in the midst of climate change. Plant biotechnology is currently limited by the cost, ease, and throughput of methods for probing plant genetics and gene expression profiles. Consequently, less than a dozen complete biosynthetic pathways are known for plant natural products that have been reconstituted heterologously, compared to the ~1000 known biosynthetic pathways in bacteria and fungi[1]. RNA interference (RNAi) is sequence-specific inhibition of gene expression at the messenger RNA (mRNA) level, and can either consist of transcriptional gene silencing (TGS) or post-transcriptional gene silencing (PTGS). In PTGS, small RNA molecules – micro (miRNA) or small interfering (siRNA) – direct enzyme complexes to degrade mRNA molecules, hence suppress their activity by preventing translation.

PTGS has shown to be a prominent tool in plants for genotype-phenotype mapping[2], discovery of new biosynthetic pathways[3], increased production of valuable small molecules[4,5], understanding the functions of genes and proteins[6], and to confer resistance to plant diseases[7,8]. One common way of utilizing PTGS in plants is to directly deliver siRNA molecules into cells. However, plants have a cell wall which presents a barrier to exogenous biomolecule delivery, whereby the plant cell wall size exclusion limit is ~ 5-20 nm[9]. Consequently, viral vectors combined with *Agrobacterium tumefaciens* delivery is the preferred method to deliver siRNA into intact plant cells. Viral vectors present the advantage of directly and strongly expressing the siRNA without relying on plant transformation, however, most viruses are limited in their host range[10], often do not

result in uniform silencing of the gene, and thus levels of silencing can vary between plants and experiments[11], and might inadvertently result in the suppression of non-target genes[12]. *Agrobacterium*-mediated delivery, similarly, is also limited to use in certain plant species, often yields random DNA integration that can adversely and unpredictably affect the cell operation[13], and can be difficult to scale or multiplex for high-throughput or multi-gene target applications, respectively[14].

While nanoparticle-mediated delivery of genes, RNAs, and therapeutics has been extensively explored in animals[15,16], their potential for plant systems remains under-studied[17]. Several prior studies take advantage of nanomaterials to deliver plasmid DNA[18-21] or proteins[22] to intact plant cells. Polymeric nanoparticles have shown promise for siRNA delivery to cell wall-free plant protoplasts, but polymeric nanoparticles have not been shown to traverse the cell wall for gene silencing in intact plant cells[10]. A recent study has shown that clay nanosheets can facilitate delivery of RNAi molecules (double-stranded RNA - dsRNA) into intact walled plant cells[23]. To our knowledge, this clay nanosheet platform is the first promising use of nanoparticles for delivery of RNAi into intact plant cells, paving the way towards future developments in plant bionanotechnology.

In this study, we demonstrate the delivery of a different but also effective RNAi molecule – siRNA – into intact cells of plant leaves using high-aspect-ratio one dimensional carbon nanomaterials: single-walled carbon nanotubes (SWNTs). SWNTs are allotropes of carbon that have a cylindrical nanostructure with diameters of 0.8-1.2 nm and lengths of 500-1000 nm. SWNTs have been shown to passively traverse the extracted chloroplast[24] and plant membranes[25] owing to several figures of merit: high

aspect ratio, exceptional tensile strength, high surface area-to-volume ratio, and biocompatibility. SWNTs are among the few nanomaterials that can be synthesized to have a smallest dimension (~ 1 nm) below the plant size exclusion limit of ~20 nm, while also providing a large cylindrical surface area from the extrusion of their 1-dimension out to ~ 500 nm. The resulting large surface area to volume ratio is thus amenable to facile loading of appreciable quantities of biological cargoes such as siRNA. In contrast, spherical nanoparticles must often exceed the plant cell wall size exclusion limit to load necessary quantities of bio-cargoes, due to the reduced scaling of the spherical nanoparticle surface area to volume. Furthermore, when bound to SWNTs, biomolecules are protected from degradation in mammalian systems[26], exhibiting superior biostability compared to free biomolecules; a phenomenon we show herein can extend to plants. Moreover, SWNTs have strong intrinsic near-infrared (nIR) fluorescence[27,28] within the biological tissue-transparency window and beyond the chlorophyll autofluorescence range, and thus enable tracking of cargo-nanoparticle complexes deep in plant tissues. Prior usage of SWNTs in plant systems is limited to studies of SWNT biocompatibility[24,29,30], sensing of small molecules[25,31,32], and for delivery of plasmid DNA for genetic transformations[21]. To-date, there has yet to be a nanoparticle-based delivery platform for siRNA molecules into intact plant cells.

Herein, we develop a SWNT-based siRNA delivery platform for the efficient silencing of an endogenous *Nicotiana benthamiana* gene in plant leaves. We show that SWNTs enable passive delivery (without external mechanical aid) and fluorescent-tracking of siRNA molecules in plant tissues. SWNTs present a non-toxic platform for siRNA delivery that uses a minimal siRNA dose to achieve silencing for up to 7 days,

whereby silencing can be sustained upon re-infiltration of the siRNA-SWNT dose. With SWNT-mediated siRNA delivery, we achieve 95% gene silencing efficiency at the mRNA level, and show a significant delay in siRNA nuclease degradation in cells, and also at the single-molecule level, through protection by SWNTs. Taken altogether, our data suggest that our SWNT-based delivery platform is scalable, facile to multiplex for multiple gene silencing targets, and species-independent[21,29,33-35]. In sum, this study establishes that SWNTs, which are below the size exclusion limit of the plant cell wall, could be a promising solution to overcome plant biomolecule delivery limitations, and could enable a variety of plant biotechnology applications based on RNAi.

Results

Preparation and characterization of siRNA-SWNTs

In this study, we aim to validate SWNTs as a passive and effective siRNA delivery and gene silencing platform for use in mature plants. To this end, we aim to silence GFP gene expression in transgenic mGFP5 *Nicotiana benthamiana* (*Nb*) plants by delivering siRNA molecules into leaves with SWNT nanocarriers. mGFP5 *Nb* plants constitutively express GFP targeted to the ER under the control of the *Cauliflower mosaic virus* 35S promoter[36] (DNA sequences for the promoter and GFP gene can be found in Supplementary Data 1). Herein, we tested two separate siRNA sequences (a-siRNA and b-siRNA) which target two different regions of the mGFP5 gene for GFP silencing (Fig. 1a).

Loading of siRNA on SWNTs was accomplished by probe-tip sonication of each siRNA single-strand (sense, and separately antisense) with pristine SWNTs for both a-siRNA and b-siRNA sequences (Fig. 1b). With this method, sense and antisense strands of siRNA were non-covalently adsorbed on SWNTs via π-π stacking of RNA nitrogen

bases with the π bonds of sp^2-hybridized carbons in SWNTs. The adsorption of RNA on SWNTs was confirmed for each sequence (a-antisense-SWNT, a-sense-SWNT, b-antisense-SWNT and b-sense SWNT) through the emergence of characteristic peaks in the individually-suspended SWNT absorbance (Fig. 1c) and nIR fluorescence emission spectra (Fig. 1d). We hypothesize and later verify that upon infiltration of an equimolar mixture of sense and antisense suspended SWNTs, these complementary siRNA strands desorb from the SWNT surface and hybridize to each other inside plant cells to form the active double-stranded siRNA silencing complex.

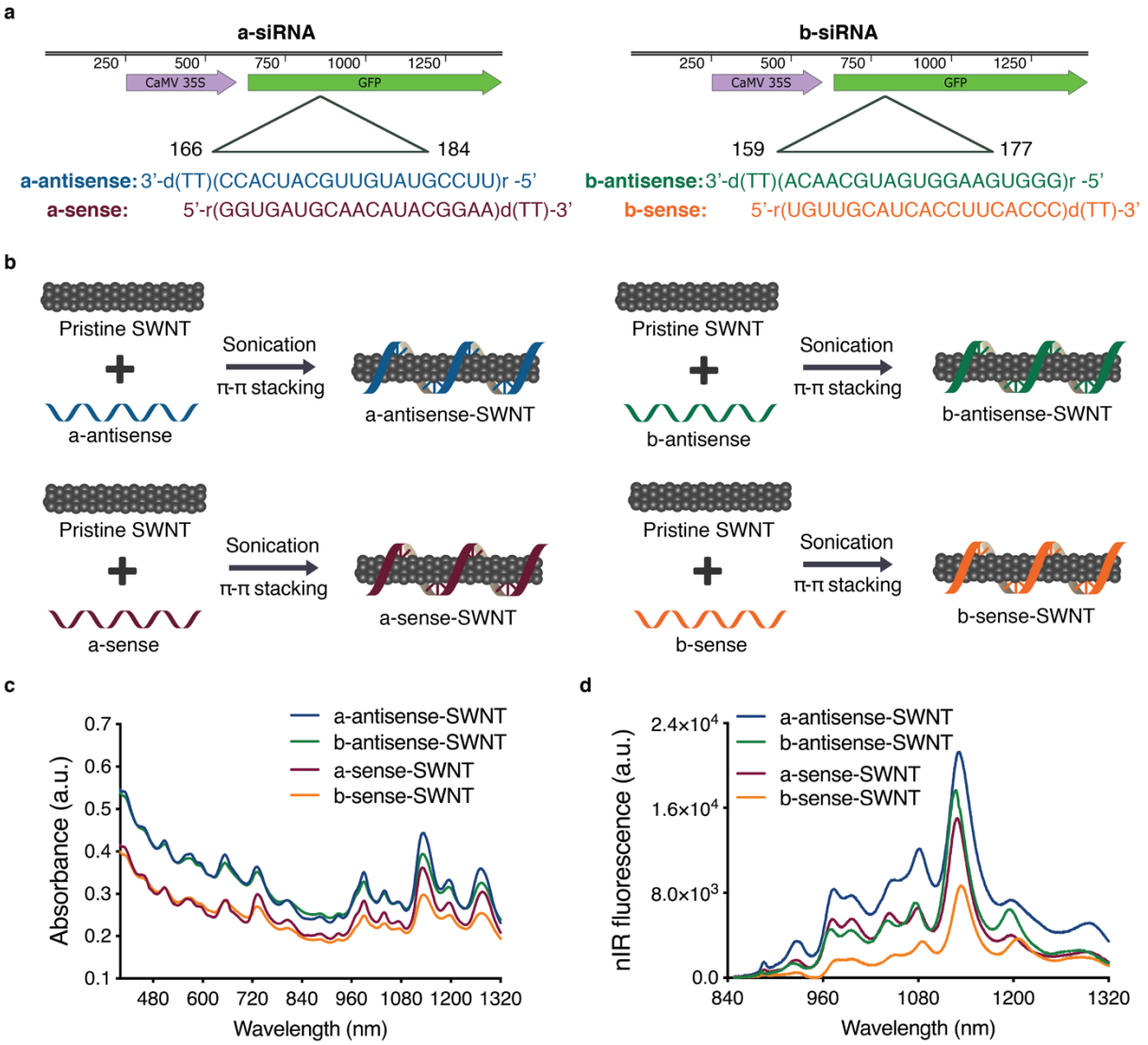

Fig. 1 siRNA-SWNT preparation and characterization. a Two sets of siRNA sequences targeting the GFP gene of transgenic mGFP5 *Nicotiana benthamiana* were separately tested in this study. Sequences on the left were chosen from Tang *et al.*[37] and sequences on the right were designed specifically for this study. **b** Suspension of pristine SWNTs with sense and antisense single-stranded RNA sequences via probe-tip sonication. **c** Absorbance spectra of RNA-SWNTs demonstrate characteristic peaks of individually suspended SWNTs with RNA strands. **d** nIR spectra of RNA-SWNTs demonstrate characteristic peaks of individually suspended SWNTs with RNA strands.

As a negative control for all siRNA silencing studies, we used SWNTs suspended with a non-targeting RNA sequence[38] (NT-SWNT, Supplementary Table 1), which is not complementary to the mGFP5 mRNA. Successful suspension of SWNTs with non-

targeting RNA sense and antisense strands was confirmed by absorbance and fluorescence spectra of individually suspended NT-SWNTs (Supplementary Fig. 1).

We first tested the internalization of RNA-SWNTs into intact mGFP5 *Nb* leaf cells. Cy3 fluorophore-tagged RNA-SWNTs (Cy3-RNA-SWNT) and Cy3 tagged free RNA (Cy3-RNA) solutions were infiltrated into the leaves of mature plants by introducing a small puncture on the abaxial surface of the leaf lamina with a pipette tip, and infiltrating each solution with a needleless syringe (Fig. 2a). Following 6 hours of incubation, infiltrated mGFP5 *Nb* leaves were imaged with confocal microscopy to quantify Cy3 fluorescence inside leaf cells and in the extracellular area. In plants, the cytosol is pushed to the cell periphery due to the presence of a large central vacuole. Leaves infiltrated with Cy3-RNA-SWNTs showed a high degree of co-localization (70% ± 8%, mean ± SD) between the intracellular (cytosolic) GFP and Cy3 fluorescence originating from the nanocarriers, which confirms efficient internalization of RNA-SWNTs into intact cells (Fig. 2b). Conversely, leaves infiltrated with Cy3-RNA show minimal co-localization between the GFP and Cy3 channels (12% ± 10%, mean ± SD), and Cy3 fluorescence is observed mostly around the guard cells, suggesting free RNA is either not able to internalize into intact plant cells efficiently or is degraded quickly (Fig. 2b). Additional confocal images of Cy3-RNA-SWNT and Cy3-RNA infiltrated leaves with representative higher and lower co-localization percentages are presented in Supplementary Fig. 2.

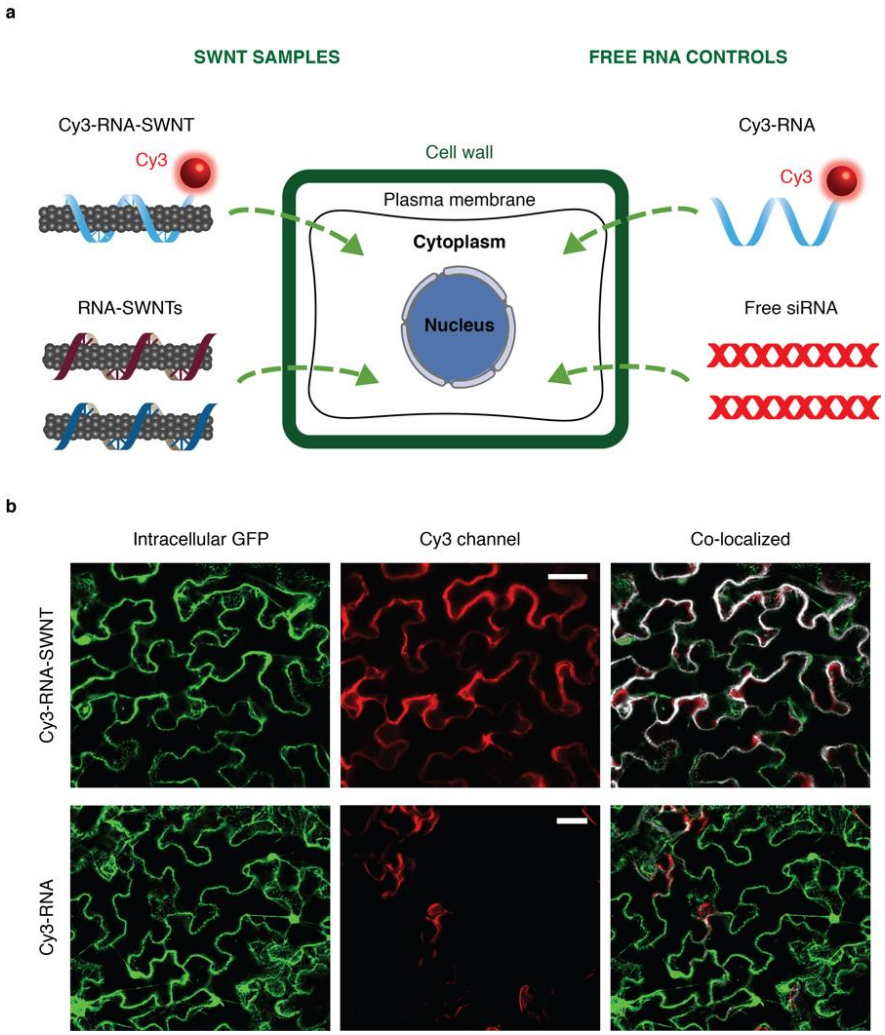

Fig. 2 RNA-SWNT internalization into transgenic mGFP5 *Nicotiana benthamiana* leaves. a Schematic showing samples tested for internalization into mGFP5 *Nb* leaves (Cy3-tagged RNA-SWNTs and Cy3-tagged free RNA as a control), and samples subsequently tested for silencing of a constitutively expressed GFP gene (RNA-SWNTs and free siRNA as a control). **b** Representative confocal images of Cy3-RNA-SWNT and Cy3-RNA infiltrated *Nb* leaves demonstrate significant co-localization between intracellular GFP and Cy3 channels for the Cy3-RNA-SWNT sample, and minimal co-localization for the free Cy3-RNA sample except around the guard cells. All scale bars are 20 µm.

In addition to confocal imaging of fluorophore tagged RNA-SWNTs, we verified internalization of SWNT nanocarriers into intact leaf cells by leveraging the intrinsic SWNT nIR fluorescence. mGFP5 *Nb* leaves were infiltrated with RNA-SWNTs or free RNA without a fluorophore (Fig. 2a). Following 6 hours of incubation, we imaged the

infiltrated leaves with a custom-built nIR microscope equipped with a Raptor Ninox VIS-SWIR 640 camera, a 721 nm SWNT excitation laser, and a white lamp and appropriate filters to image GFP (see Methods). In leaves infiltrated with RNA-SWNTs, commensurate with Cy3-tagged confocal imaging results, we observe a high degree of co-localization between intracellular GFP and the nIR fluorescence of SWNTs (Supplementary Fig. 3a), further substantiating efficient internalization of SWNTs into intact plant cells. No co-localization was observed in leaves treated with unlabeled free RNA. The internalization of SWNT nanocarriers into plant cells is also supported by the solvatochromic shift in the nIR fluorescence spectra of RNA-SWNTs upon cell internalization. Compared to as-prepared RNA-SWNTs, the nIR fluorescence spectra of RNA-SWNTs shows a 6-nm solvatochromic shift in the SWNT nIR fluorescence emission spectra upon cell membrane crossing, characteristic of a biomolecule adsorption-induced change in the SWNT dielectric environment[39] (Supplementary Fig. 3b). All internalization studies were performed with a-antisense-SWNT suspension as a representative strand to demonstrate the internalization ability of single-stranded RNA loaded SWNTs into intact walled plant leaf cells.

After confirming that siRNA adsorbed SWNTs can efficiently be uptaken by plant cells, we analyzed the thermodynamics of sense and antisense strand hybridization, and their subsequent propensities for desorption from the SWNT surface in the extracellular and intracellular conditions. According to our calculations (Supplementary Information), in the *in vitro* and extracellular area of the leaf tissue, sense and antisense strand hybridization and desorption from the SWNT surface is not thermodynamically favorable ($\Delta G>0$), due to a high free energy cost of bare SWNTs in an aqueous environment (Fig.

3a). This unfavorable RNA desorption energy facilitates maintenance of intact RNA-SWNT conjugates in the extracellular environment until RNA-SWNTs enter cells. Once intracellular, sense and antisense strand hybridization and desorption from the SWNT surface is thermodynamically favorable ($\Delta G<0$) because intracellular proteins, lipids, and other membrane and cytosolic biomolecules can occupy the SWNT surface and lower the associated free energy costs of RNA desorption (Fig. 3b). Cytosolic biomolecule adsorption to intracellular SWNT was experimentally confirmed with a 6-nm solvatochromic shift in the SWNT nIR fluorescence spectra following plant cell infiltration and cellular internalization [39] (Supplementary Fig. 3b).

Once desorbed from SWNTs and hybridized, double-stranded active siRNA can merge with the gene silencing complex, whereby the antisense strand of siRNA directs the complex to the endogenous target mRNA. Upon hybridization of the antisense strand with the complementary target mRNA sequence, Argonaute 2 (AGO2), a protein in the gene silencing complex, cleaves the target mRNA and prevents translation of GFP proteins (Fig. 3b).

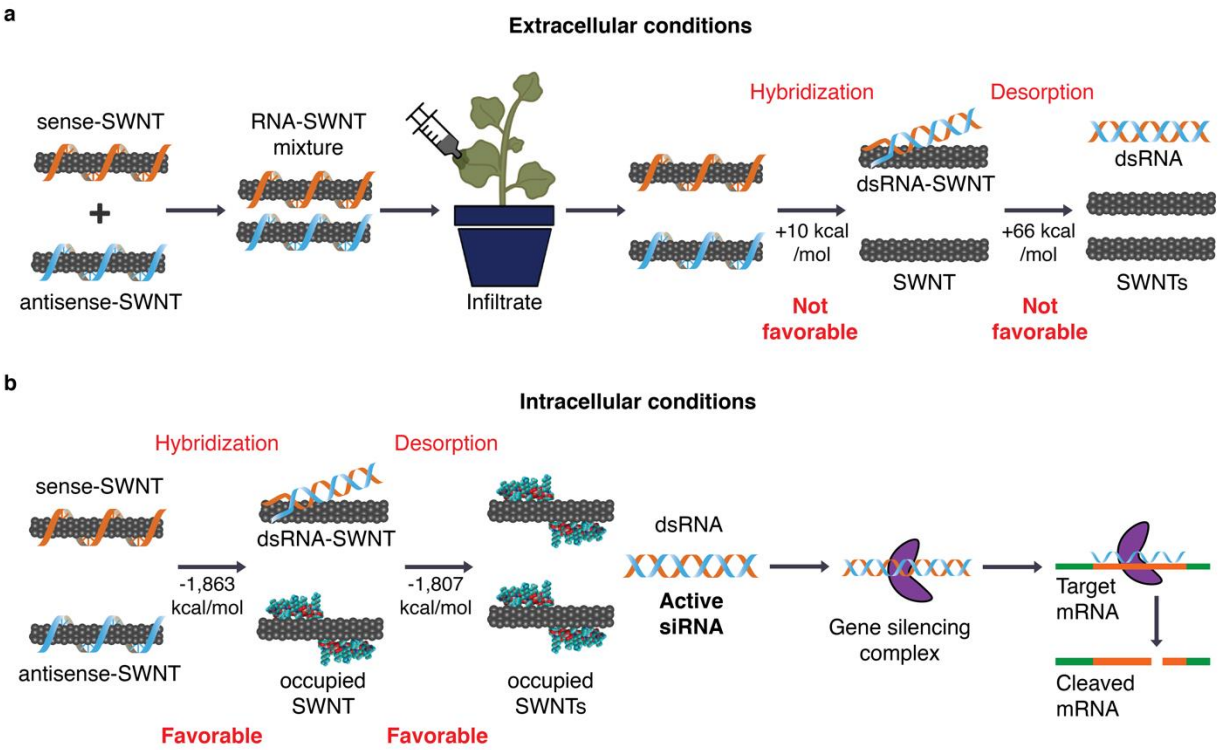

Fig. 3 Thermodynamic analysis of RNA hybridization and desorption from SWNTs in extracellular and intracellular conditions, and proposed gene silencing mechanism. a An equimolar mixture of sense-SWNT and antisense-SWNT suspensions are infiltrated into transgenic *Nb* leaves with a needleless syringe. In the extracellular area of leaf tissue, RNA hybridization and desorption from SWNTs is not thermodynamically favorable due to the high free energy cost of bare SWNTs. **b** Inside cells, RNA hybridization and desorption from SWNTs is thermodynamically favorable because molecules can occupy the bare SWNT surface and lower the RNA desorption free energy cost. Upon desorption from SWNTs, double-stranded active siRNA assembles with the gene silencing complex and complexes with target mRNA for cleavage and gene silencing.

Following verification of SWNT internalization and thermodynamically-favorable formation of active siRNA complexes in plant cells, we next infiltrated transgenic mGFP5 *Nb* leaves with RNA-SWNTs and control solutions to determine the gene silencing efficiency of this platform. Silencing studies were conducted with the following samples at 100 nM final siRNA concentration (when applicable): non-treated leaves, NT-SWNT (non-targeting), free siRNA, a-siRNA-SWNT, and b-siRNA-SWNT (See Supplementary

Table 1 for sequences). Transgenic *Nb* leaves that constitutively express GFP were imaged via confocal microscopy to quantify GFP silencing at the protein level. Representative confocal images of the leaves 2-days post-infiltration reveals that both a-siRNA-SWNTs and b-siRNA-SWNTs lead to significant reduction of GFP in cells, whereas GFP expression in leaves infiltrated with NT-SWNT and free siRNA appears similar to GFP expression in non-treated leaves (Fig. 4a). Quantification of GFP fluorescence intensity from the confocal images of NT-SWNTs and a-siRNA-SWNTs (see Methods) reveals that a-siRNA-SWNT infiltrated leaves have 38% ± 3.2% (mean ± SD) less GFP protein 3-days post-infiltration compared to the NT-SWNT infiltrated leaves. At 7-days post-infiltration, a-siRNA-SWNT shows roughly the same amount of GFP, 106.6 ± 4.1% (mean ± SD), as NT-SWNT infiltrated leaves (Fig. 4b), as expected since gene silencing with siRNA is a transient process. GFP silencing with a-siRNA-SWNT was also verified with a Western blot analysis, where GFP extracted from the *Nb* leaves infiltrated with a-siRNA-SWNT is 42.6% ± 2.8% (mean ± SD) less than GFP extracted from NT-SWNT infiltrated leaves both at 1 and 2-days post-infiltration (Fig. 4c).

We corroborated the GFP reduction results obtained with confocal imaging and Western blot analysis by performing quantitative PCR (qPCR) at the mRNA transcript level. One day after infiltration of leaves with NT-SWNT, free siRNA, a-siRNA-SWNT, and b-siRNA-SWNT, we extracted total mRNA from the leaves and quantified the GFP mRNA transcript levels in each sample at Day 1 and 7. qPCR demonstrates that NT-SWNT and free siRNA infiltrated leaves have the same amount of GFP mRNA transcript as the non-treated leaf, whereby a-siRNA-SWNT and b-siRNA-SWNT infiltrated leaves show 95% ± 4.1% (mean ± SD) and 92% ± 6.2% (mean ± SD) reduction in the GFP mRNA transcript

levels at Day 1, respectively (Fig. 4d). Similar to the confocal results, we found that mRNA transcript levels return back to the baseline levels as observed in non-treated leaves by Day 7 in all samples as a result of transient silencing (Fig. 4d). Additionally, we show we can recover GFP silencing at Day 7 by up to 71% ± 2.9% (mean ± SD) by re-infiltrating the leaf with second 100 nM a-siRNA-SWNT dose at Day 5 (Fig. 4e).

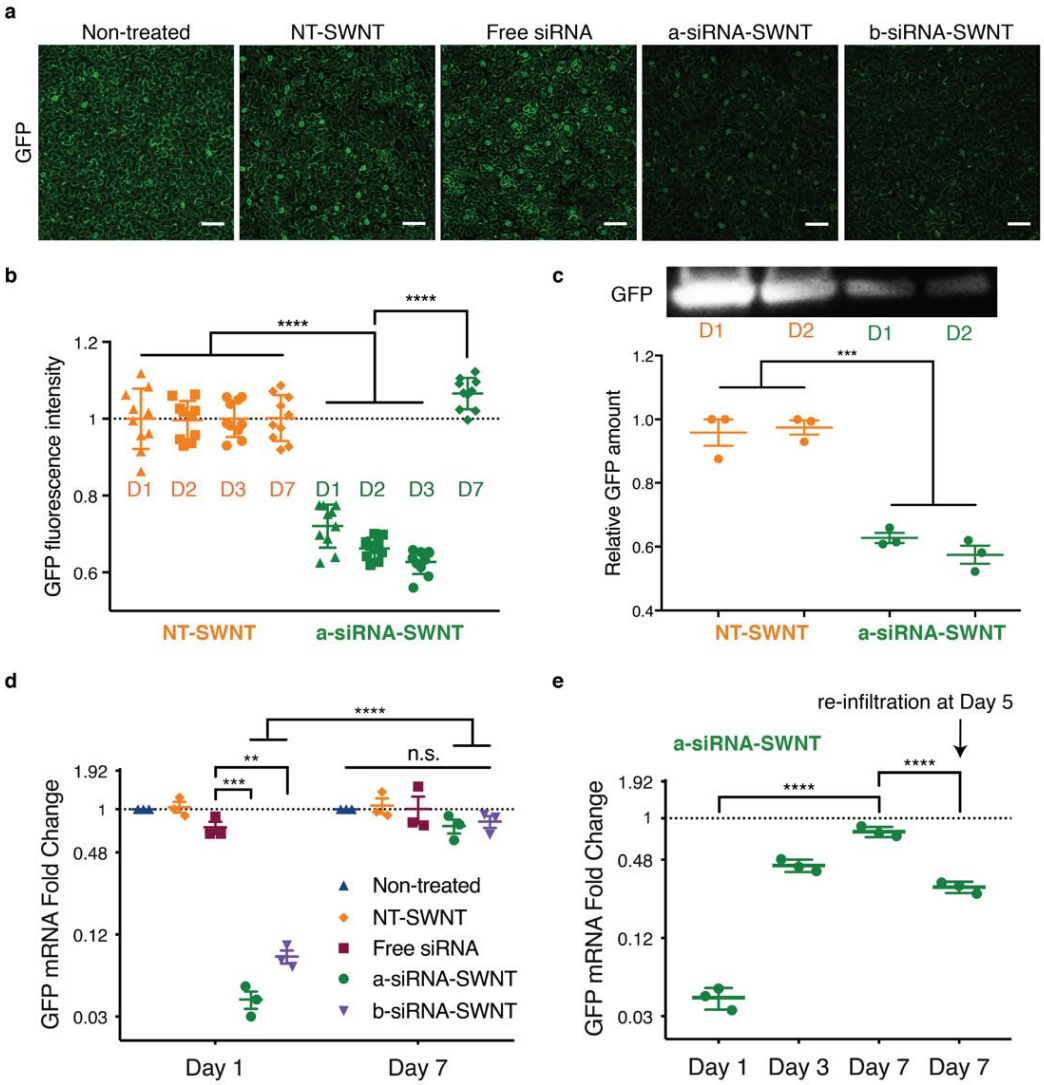

Fig. 4 GFP gene silencing with RNA-SWNTs at the mRNA transcript and protein level. a Representative confocal microscopy images of non-treated, NT-SWNT, free siRNA, a-siRNA-SWNT, and b-siRNA-SWNT infiltrated transgenic *Nb* leaves 2-days post-infiltration. Scale bars, 100 µm. **b** Quantitative fluorescence intensity analysis of confocal images for NT-SWNT and a-siRNA-SWNT at 1, 2, 3 and 7-days post-infiltration. ****P < 0.0001 in one-way ANOVA. Error bars indicate s.d. (n = 10). **c** Representative

Western blot for GFP extracted from NT-SWNT and a-siRNA-SWNT infiltrated *Nb* leaves 1 and 2 days post-infiltration, and quantification of GFP protein. ***P = 0.0001 in one-way ANOVA and error bars indicate s.e.m (n = 3). **d** qPCR analysis for GFP mRNA fold change at Day 1 and 7 post-infiltration for all samples tested. **P = 0.0016, ***P = 0.0008 and ****P < 0.0001 in two-way ANOVA (n.s: non-significant) All error bars indicate s.e.m. (n = 3). **e** qPCR analysis for GFP mRNA fold change at Day 1, 3, 7 and Day 7 with re-infiltration at Day 5 for a-siRNA-SWNT treated *Nb* leaf sample. ****P < 0.0001 in one-way ANOVA and all error bars indicate s.e.m. (n = 3). All qPCR data for GFP expression are normalized with respect to housekeeping gene Elongation Factor 1 (EF1), and a control sample of a non-treated leaf.

It is likely that SWNT scaffolding improves internalization of siRNA and also protects siRNA from degradation once intracellular. To explore this hypothesis, we performed single molecule total internal reflection fluorescence (smTIRF) microscopy to probe single siRNA strand susceptibility to degradation by RNase A when adsorbed on SWNTs, compared to single free siRNA. To do so, we labeled the a-antisense strand of GFP siRNA with a 5' terminal Cy3 fluorophore, and immobilized RNA-Cy3 and RNA-Cy3-SWNTs onto parallel channels of a microfluidic slide (see Methods). We measured the Cy3 fluorescence in each channel before and after treatment with RNase A, whereby percent decrease in the number of Cy3 molecules was used as a proxy for the percent siRNA degraded (Fig. 5a). Our TIRF results show that 98% ± 0.3% (mean ± SD) of the initial Cy3-RNA immobilized on the channel surface is degraded after incubation with RNase A, whereas only 16% ± 4.9% (mean ± SD) of Cy3-RNA is degraded when it is bound to SWNTs, suggesting that SWNTs protect the siRNA cargo from enzymatic degradation inside cells (Fig. 5b). Negative controls in which only salt buffer is flown through, or empty BSA-passivated channels, do not show appreciable changes in fluorescence or fluorescence counts, respectively (Supplementary Fig. 4).

Intracellular stability of RNA-SWNTs and free RNA was also assessed by incubating RNA-SWNT conjugates with total proteins extracted from plant leaves (i.e.

plant cell lysate). Agarose gel electrophoresis of free RNA vs. RNA-SWNTs incubated in plant cell lysate for 1, 3, 6, 12, and 24 hours demonstrate that free RNA is degraded significantly faster in cells compared to RNA adsorbed on SWNTs (Fig. 5c). Band intensity quantification of agarose gel reveals that upon starting with 200 ng RNA, free RNA is completely degraded within 12 hours, whereas the RNA on the SWNTs is only completely degraded after 24 hours (Fig. 5d and 5e), which corresponds to a 12 hour increase in the residence time of siRNA in cells when delivered through SWNTs that could give rise to prolonged and increased silencing efficiency.

To test whether SWNT nanocarriers are biocompatible, we undertook plant toxicity and tissue damage tests. Specifically, for toxicity studies, we performed qPCR analysis of respiratory burst oxidase homolog B (NbrbohB) upregulation (Fig. 5f), a known stress gene representing many different types of stress conditions (mechanical, light, heat, biotic, etc.) in *Nb* plants[40]. Quantification of NbrbohB expression shows that SWNT-treated areas in leaves do not upregulate NbrbohB compared to adjacent areas within the same leaves treated only with buffer, whereby the positive control for toxicity, 1% SDS, upregulates the stress gene by 6-fold 3 hours post-infiltration (Fig. 5f). We also analyzed leaf tissue damage visually and via confocal microscopy, which again showed no sign of tissue damage in SWNT-infiltrated leaves (Supplementary Fig. 5). Our analysis concludes that the SWNT-based delivery platform is biocompatible and does not induce toxicity or tissue damage to mature plants with the conditions used in the present study.

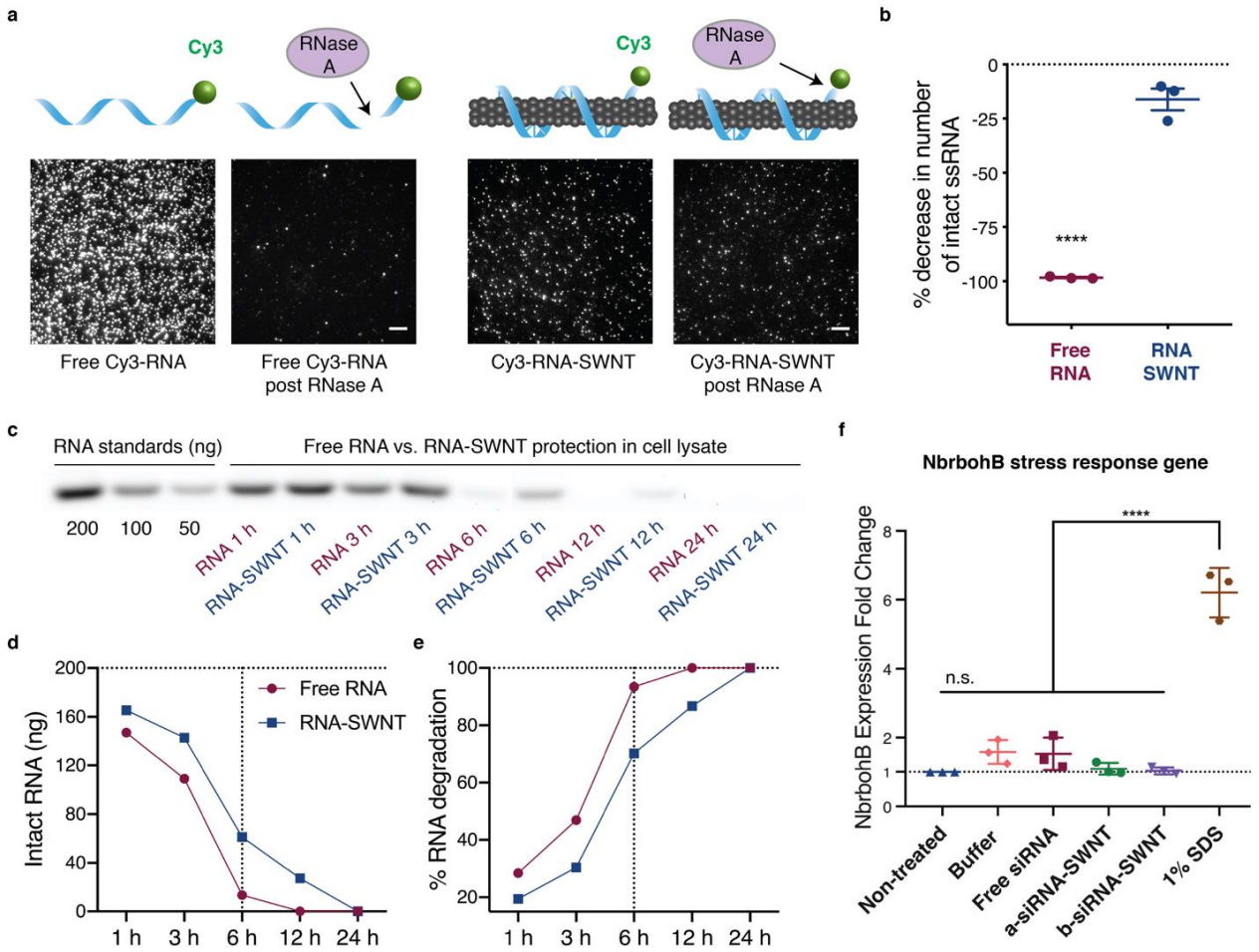

Fig. 5 RNA protection from enzymatic degradation on SWNTs and SWNT toxicity analysis. a Single molecule TIRF microscopy of Cy3-labeled RNA and Cy3-labeled RNA-SWNTs before and after incubation with RNase A. Scale bars, 5 µm. **b** Quantification of % decrease in number of intact RNA molecules upon RNase A treatment of free RNA and RNA-SWNT. Error bars indicate s.e.m. (n = 3). ****$P < 0.0001$ in two-tailed unpaired t-test. **c** Agarose gel electrophoresis of free RNA and RNA-SWNTs incubated in plant cell lysate solution for 1, 3, 6, 12, and 24 hours. **d** Quantification of intact RNA from the agarose gel in part c for free RNA and RNA on SWNTs**. e** Quantification of % RNA degradation from the agarose gel in part c for free RNA and RNA on SWNTs**. f** qPCR analysis of NbrbohB, a known stress gene in *Nb* plants, to test SWNT toxicity, following a 3-hour exposure to samples. ****$P < 0.0001$ in one-way ANOVA and error bars indicate s.e.m. (n = 3).

Discussion

Nanoparticles have shown much promise for plasmid[21] and protein[22] delivery to plants, motivating their use for plant delivery of RNAi, as has proven quite fruitful for human

therapeutics. We demonstrate here that high-aspect-ratio one dimensional SWNTs can successfully deliver siRNA molecules to efficiently silence a GFP gene in transgenic *Nicotiana benthamiana* mature plant leaves, through a combination of i) effective intracellular delivery and ii) protection of the siRNA cargo from nuclease degradation. We found that RNA adsorbed SWNTs internalize into mature walled plant cells with high efficiency within 6 hours in contrast to free RNA internalization which is minimal. We further found that π-π adsorption of siRNA on the SWNT surface delays intracellular siRNA degradation and thus prolongs silencing.

Current methods of siRNA delivery with nanoparticles focus on loading the active RNA duplexes on particles through charge interactions[10,41], which can cause immediate release of RNA upon interaction with plant tissue and faster degradation of RNA duplexes before they reach the cytosol. Here, we developed a platform for siRNA delivery using nanoparticles, uniquely suited for cellular delivery in plant tissues with intact cell walls. This platform utilizes SWNTs, to which single-stranded sense and antisense siRNA are adsorbed separately, enabling thermodynamically-favorable siRNA hybridization once intracellular for subsequent gene silencing mechanisms. We show that RNA is protected from degradation for up to 24 hours when adsorbed to SWNTs, whereas free RNA is almost completely degraded by 6-12 hours. We show a similar siRNA protection phenomenon with single-molecule TIRF microscopy of individual siRNA molecules either free or adsorbed to SWNTs. With this SWNT loading and delivery platform, we achieve transient and DNA-free silencing of genes in mature plant leaves with a low siRNA-SWNT dose, showing silencing efficiencies of up to 95% that persist for 7 days. We further show

that it is possible to retain gene silencing for longer periods of time with a re-infiltration of another siRNA-SWNT dose at day 5.

The commonly used cationic nanoparticles for the delivery of negatively charged siRNA through electrostatic interactions have shown appreciable cellular toxicity to cells for certain effective concentrations and/or charge densities[42]. The pristine non-charged SWNT surface eliminates this problem and makes it possible to scale-up the delivery of siRNA for higher doses or systemic administration. Additionally, the platform could be adapted to loading multiple siRNA sequences to multiplex gene silencing targets by delivering a mixture of SWNTs suspended with multiple siRNA sequences or loading a single SWNT sample with multiple siRNA sequences. Furthermore, SWNT internalization into plants is species-independent and can be used with monocots, non-model species, or hard-to-transform species[21].

Given aforementioned advantages, we believe that there is a broad range of applications of our RNAi platform. The process of RNA adsorption to SWNTs is based on π-π adsorption and thus agnostic to the function of the RNA cargo. Additional to the more traditional applications of RNAi in plants, such as disease/virus resistance, discovery of biosynthetic pathways, increasing the yield of small-molecule production, and understanding protein functions, SWNT-mediated gene silencing could also be used for efficient and DNA-free delivery of other synthetic ribonucleic acids. For instance, SWNTs could aid nuclease-based genome editing in plants by delivery of single guide RNAs (sgRNAs) and/or messenger RNAs (mRNAs) for controlled and transient nuclease expression and subsequent genome editing. Another potential application of SWNT-based RNA delivery is for increasing homology-directed repair (HDR) rates in plants for

gene knock-in applications, which could possibly be achieved by suppressing the expression of the genes required for competitive non-homologous end joining (NHEJ) repair pathways[43]. As the efficient suppression of these genes is only desirable for the few-day time window in which genome editing takes place, our SWNT-mediated gene silencing platform could enable such control over transient siRNA delivery. As such, SWNT-based delivery of polynucleic acids such as RNAs is a useful addition to the plant biotechnology toolkit.

Materials and Methods

Procurement and preparation of chemicals and nanomaterials. Super purified HiPCO SWNTs (Lot # HS28-037) were purchased from NanoIntegris, and SWNTs samples were extensively purified before use[44]. Single-stranded RNA strands, Cy3-tagged single-stranded RNA strands and all primer sequences were purchased from IDT and dissolved in 0.1M NaCl before use. 100K MWCO Amicon spin filters were purchased from Fisher Scientific. The following chemicals were purchased from Sigma-Aldrich: sodium dodecyl sulfate (molecular biology grade), sodium chloride, Tris/HCl, EDTA, NP-40, glycerol, BSA-Biotin and NeutrAvidin. RNAse A was purchased from Takara Bio. All PCR reagents and materials, and molecular biology grade agarose were purchased from Bio-Rad. UltraPure DNase/RNase-free distilled water from Invitrogen was used for qPCR and PCR experiments, and EMD Millipore Milli-Q water was used for all other experiments.

Plant growth. Transgenic mGFP5 *Nicotiana benthamiana* seeds were kindly provided by the Staskawicz Lab, UC Berkeley. The seeds were germinated and grown in SunGro Sunshine LC1 Grower soil mix for four to six weeks before experiments in a growth chamber, 12-hour light at 24°C and 12-hour dark at 18°C cycle. All experiments were done with intact leaves attached to plants, where plants were incubated in the growth chamber until the time of data collection.

RNA-SWNT and Cy3-RNA-SWNT preparation. SWNTs were suspended with single-stranded RNA polymers or Cy3-tagged single-stranded RNA sequences through probe-tip sonication as previously

described[45]. See **Supplementary Table 1** for all RNA sequences used in this study. Briefly, RNA was dissolved at a concentration of 100 mg/mL in 0.1 M NaCl. 20 μL of this RNA solution was aliquoted into 980 μL 0.1 M NaCl and 1 mg HiPCO SWNTs was added. The mixture was bath sonicated for 10 min, followed by probe-tip sonication with a 3-mm tip at 50% amplitude (~7W) for 30 min in an ice bath. The resulting solution rested at room temperature for 30 minutes before centrifugation at 16,100g for 1 h to remove unsuspended SWNT aggregates and metal catalyst precursor. Unbound (free) RNA was removed via spin-filtering (Amicon, 100 K) 10-15 times and the concentration of RNA-SWNTs was determined by measuring the SWNT absorbance at 632 nm. Absorbance spectra of RNA-SWNTs were collected with Shimadzu UV-3600 Plus, and fluorescence spectra of RNA-SWNTs were collected with a near-infrared spectrometer (Princeton Instruments IsoPlane 320 coupled to a liquid nitrogen-cooled Princeton Instruments PyLoN-IR 1D array of InGaAs pixels).

Infiltration of leaves with RNA-SWNTs and control solutions. Healthy and fully-developed leaves from mGFP5 *Nicotiana benthamiana* (4-6 weeks old) plants were selected for experiments. A small puncture on the abaxial surface of the leaf lamina was introduced with a pipette tip, and ~200 μL of the RNA-SWNT solution (or of any control solution) was infiltrated from the hole with a 1 mL needleless syringe by applying a gentle pressure, with caution not to damage the leaf.

Internalization imaging with confocal and nIR fluorescence microscopy. The a-antisense siRNA strand was utilized in the internalization study. After infiltration, plants with attached infiltrated leaves were left in the plant growth chamber to allow for internalization for 6 h, and imaged with either confocal microscopy to track Cy3-tagged RNA-SWNTs in leaves or with nIR microscopy to directly track nIR fluorescence of RNA-SWNTs. A Zeiss LSM 710 confocal microscope was used to image the plant tissue with 488 nm laser excitation with a GFP filter cube to detect intracellular GFP, and 543 nm laser excitation with an appropriate filter cube to detect Cy3 fluorescence. The emission window of Cy3 was adjusted to 550-600 nm to avoid crosstalk between Cy3 and leaf chlorophyll autofluorescence. nIR images of RNA-SWNT leaf internalization were captured using a custom-built microscope equipped with a Raptor Ninox VIS-SWIR 640 camera. A 1050-nm long pass filter was used to avoid chlorophyll autofluorescence, and a white lamp with an appropriate filter cube was used to image GFP. GFP and Cy3 (or nIR) images were analyzed with the ImageJ co-localization program to demonstrate internalization of RNA-SWNTs into cells.

Confocal imaging for silencing and quantitative fluorescence intensity analysis of GFP expression. mGFP5 *Nb* leaves were infiltrated with NT-SWNT, free siRNA, a-siRNA-SWNT, and b-siRNA-SWNT at the same RNA concentration of 100 nM. Infiltrated plant leaves were prepared for confocal imaging 1, 2, 3, and 7-days post-infiltration by cutting a small leaf section of the infiltrated leaf tissue, and inserting the tissue section between a glass slide and cover slip of #1 thickness. 100 µL water was added between the glass slide and cover slip to keep the leaves hydrated during imaging. Confocal image data were analyzed to quantify GFP expression across samples. For each sample, 10 technical replicates (10 non-overlapping confocal field of views from each leaf) were collected. Each field of view was analyzed with custom ImageJ analysis to quantify the GFP fluorescence intensity value for that field of view, and all 10 field of views were then averaged to obtain a mean fluorescence intensity value for that sample. For each sample, mean fluorescence intensity value was normalized with respect to the mean GFP fluorescence intensity of a non-treated leaf. The same imaging parameters and quantification analyses were applied to samples imaged on different days.

Quantitative Western blot experiments and data analysis. Infiltrated plant leaves were harvested 24 and 48 h post-infiltration and ground in liquid nitrogen to recover dry frozen powders. The frozen powders were transferred to a tube with pre-prepared lysis buffer containing 10 mM Tris/HCl (pH 7.5), 150 mM NaCl, 1 mM EDTA, 0.1% NP-40, 5% glycerol, and 1% Cocktail. After lysis at 4℃ overnight, the tube was centrifuged at 10,000 rpm for 15 minutes and the supernatant containing whole proteins was collected into a new tube. After quantification of the total extracted proteins by a Pierce 660 nm Protein Assay (Thermo, Prod# 22660), 0.5 µg of normalized total proteins from each sample were analyzed by 12% SDS–PAGE and blotted to a PVDF membrane. The membrane was blocked for 1 hour using 7.5% BSA in PBST (PBS containing 0.1% Tween20) buffer and incubated overnight at 4°C with the primary GFP antibody as required (1:2000 dilution, Abcam, ab290). After extensive washing, the corresponding protein bands were probed with a goat anti-rabbit horseradish peroxidase-conjugated antibody (1:5000 dilution, Abcam, ab205718) for 30 min. The membrane was then developed by incubation with chemiluminescence (Amersham ECL prime kit) plus and imaged by ChemiDoc™ XRS+ System. The intensity of GFP bands were quantified with ImageJ software.

Quantitative PCR (qPCR) experiments for gene silencing. Two-step qPCR was performed to quantify GFP gene silencing in transgenic *Nb* plants with the following commercially-available kits: RNeasy plant mini kit (QIAGEN) for total RNA extraction from leaves, iScript cDNA synthesis kit (Bio-Rad) to reverse transcribe total RNA into cDNA, and PowerUp SYBR green master mix (Applied Biosystems) for qPCR. The target gene in our qPCR was mGFP5 (GFP transgene inserted into *Nb*), and EF1 (elongation factor 1) as our housekeeping (reference) gene. Primers for these genes can be found in **Supplementary Table 1.** An annealing temperature of 60˚C was used for qPCR, which we ran for 40 cycles.

qPCR data was analyzed by the ddCt method[46] to obtain the normalized GFP gene expression-fold change with respect to the EF1 housekeeping gene and control sample (non-treated leaf). For each sample, qPCR was performed as 3 technical replicates (3 reactions from the same isolated RNA batch), and the entire experiment consisting of independent infiltrations and RNA extractions from different plants was repeated 3 times (3 biological replicates).

Single molecule TIRF to image RNA protection by SWNTs. The a-antisense siRNA strand was utilized in this assay. 10 μM 5' labelled Cy3-RNA was added to an equal mass of SWNTs. The RNA-SWNT suspension and removal of unbound RNA followed the same protocol as described in 'Quantitative PCR (qPCR) experiments for gene silencing'. The positive control comprised of the same sequence that was 5' Cy3 labeled, and 3' biotin labeled. 6-channel μ-slides (ibidi, μ-Slide VI 0.5 Glass Bottom) were initially washed by pipetting 100 μL of 100 mM sterile NaCl solutions into one reservoir and removing 60 μL the other end, leaving just enough solution to fully wet the channel. Each subsequent step involved depositing the desired solution volume into the reservoir and removing the equivalent volume from the other end of the channel. Slide preparation was done as described by Kruss and Landry *et al.*[47] with some modifications. Briefly, 50 μL of 0.25 mg/mL BSA-Biotin was added to coat the surface of the glass slide for 5 minutes. Next, 50 μL of 0.05 mg/mL NeutrAvidin was added, followed by 50 μL of 1.0 mg/L RNA-SWNT, which non-specifically adsorbs to NeutrAvidin. For the positive control, 50 μL of 200 pM biotinylated Cy3-RNA was added in place of RNA-SWNT. The addition of each component comprised of a 5-minute incubation period, followed by flushing the channel with 50 μL of NaCl solution to remove specimens that were not surface-immobilized. Each channel was exposed to 50 μL of 10 μg/mL RNase A for 15 minutes at room temperature.

The reaction was stopped by rinsing the channel with 50 μL NaCl solution. Slides were imaged with a Zeiss ELYRA PS.1 microscope immediately following incubation with RNase A.

RNA protection gel assay. Total proteins (including nucleases) were extracted from *Nb* leaves by grinding in liquid nitrogen to recover dry frozen powders. The frozen powders were transferred to a microcentrifuge tube with pre-prepared lysis buffer containing 400 μL of 10 mM Tris/HCl (pH 7.5), 150 mM NaCl, 1 mM EDTA, 0.1% NP-40, 5% glycerol, and 1% Cocktail and vortexed briefly to mix well. After lysis at 50℃for 5 minutes, the tube was centrifuged at 10,000 rpm for 30 minutes and the supernatant containing whole proteins was collected to a new tube. Total protein extract was quantified by a Pierce 660 nm Protein Assay (Thermo, Prod# 22660). 200 ng free RNA and RNA-SWNTs (carrying 200 ng RNA) were each incubated with cell lysate proteins obtained from one *Nb* leaf to mimic the intracellular degradation conditions for 1, 3, 6, 12, and 24 hours.

Following incubation, all RNA was desorbed from SWNTs at 95˚C for 1 hour in the presence of 2% SDS and 1.5 M NaCl. Desorbed RNA and cell lysate treated free RNA were run on a 1% agarose gel with RNA standards of known quantity (200, 100, and 50 ng) to measure the intact versus degraded RNA in each sample lane. RNA amounts on the agarose gel were quantified by using band intensity as a proxy (ImageJ Gel Analyzer) and normalized with the lanes containing known RNA quantities.

Plant toxicity analysis. To test for plant stress and toxicity, the expression level of an oxidative stress gene (NbRbohB)[40] in *Nb* leaves was measured through qPCR (primer sequences in **Supplementary Table 1**). The samples tested for toxicity were: buffer (0.1 M NaCl), free siRNA, a-siRNA-SWNT, b-siRNA-SWNT and 1% SDS (as a positive toxicity control), and the qPCR was performed 3-hours after the infiltration of these samples. EF1 was again measured as a housekeeping gene and an annealing temperature of 60˚C was used for qPCR, which we ran for 40 cycles .The ddCt method was used to obtain the normalized NbRbohB expression-fold change with respect to the EF1 housekeeping gene and control sample (non-treated leaf).

Statistics and data analysis.

GFP silencing confocal data. N = 10 technical replicates (10 different fields of view from the same leaf per sample infiltration) were imaged. Confocal images reported in Figure 4a are representative images chosen from 10 replicates of Day 2 data. Data are expressed as each mean from the 10 replicates together with

error bars indicating standard deviation. Significance is measured with one-way ANOVA with Tukey's multiple comparisons test. In Figure 4b, F = 124.3 and $P < 0.0001$.

Western blot experiment. N = 3 replicates are independent experiments, and Figure 4c denotes the results from a representative blot. Relative GFP amount data determined from the Western blot are expressed as mean from the 3-independent experiments together with error bars indicating standard error of the mean. Significance is measured with one-way ANOVA with Tukey's multiple comparisons test. F = 54.65, NT-SWNT vs. a-siRNA-SWNT $P = 0.0001$.

qPCR experiments. For GFP mRNA fold change experiments in Figure 4d, N = 3 replicates are independent experiments, starting with RNA extraction from different leaves through the qPCR amplifications. Each qPCR reaction in 3 independent experiments is performed in triplicate. GFP mRNA fold change data are expressed as each mean from the 3-independent experiments together with error bars indicating standard error of the mean. Significance is measured with two-way ANOVA with Sidak's multiple comparisons test. Free siRNA vs. a-siRNA-SWNT $P = 0.0008$, Free siRNA vs. b-siRNA-SWNT $P = 0.0016$, and siRNA-SWNT Day 1 vs. Day 7 $P < 0.0001$.

For qPCR results reported in Figure 4e, N = 3 replicates are independent experiments; 3 separate leaves infiltrated per sample and each measured with qPCR. Each sample in each independent experiment consisted of 3 technical replicates of the qPCR reaction. Data are expressed as each mean from the 3-independent experiments together with error bars indicating standard error of the mean. Significance is measured with one-way ANOVA with Tukey's multiple comparisons test. F = 143.7, Day 1 vs. Day 7 $P = < 0.0001$, and Day 7 vs. Day 7 (re-inf. at Day 5) $P = < 0.0001$.

smTIRF microscopy data. For each sample, N = 3 replicates are 3 channels on a microfluidic slide that were prepared independently. Each channel was imaged to obtain 30 fields of views (technical replicates). In Figure 5b, data are expressed as each mean from the 3-independent channels together with error bars indicating standard error of the mean. Significance is measured with a two-tailed unpaired t-test. F = 303.7 and $P < 0.0001$.

Toxicity qPCR data. N = 3 replicates are independent experiments with separate infiltrations of SWNT solutions for each replicate. For the toxicity plot in Figure 5f, 1% SDS vs. all other samples $P < 0.0001$ in one-way ANOVA with Tukey's multiple comparisons test, F = 82.95.

Data Availability

The DNA sequence of the GFP gene silenced in this study is added as Supplementary Data 1 file in the FASTA format. The data that support the plots within this paper and other findings of this study are available from the corresponding author upon reasonable request.

Acknowledgements

We acknowledge support of a Burroughs Wellcome Fund Career Award at the Scientific Interface (CASI), a Stanley Fahn PDF Junior Faculty Grant with Award # PF-JFA-1760, a Beckman Foundation Young Investigator Award, a USDA AFRI award, a USDA NIFA award, and an FFAR New Innovator Award (M.P.L). M.P.L. is a Chan Zuckerberg Biohub investigator. G.S.D. is supported by a Schlumberger Foundation Faculty for the Future Fellowship. We acknowledge the support of UC Berkeley Molecular Imaging Center, the QB3 Shared Stem Cell Facility, and the Innovative Genomics Institute (IGI).

Author contributions

G.S.D. and M.P.L. conceived of the project, designed the study, and wrote the manuscript. G.S.D. performed the majority of experiments and data analysis. H.Z. performed Western blot studies and helped with qPCR experiments. N.S.G. performed TIRF experiments and analyzed TIRF data. R.C. prepared some of the RNA-SWNT suspensions used in the studies. All authors have edited and commented on the manuscript, and have given their approval of the final version.

Correspondence and requests for materials should be addressed to M.P.L.

Competing interests: The authors declare no competing interests.

References

1. Lau, W. & Sattely, E. S. Six enzymes from mayapple that complete the biosynthetic pathway to the etoposide aglycone. *Science* **349**, 1224-1228 (2015).
2. Casacuberta, J. M. *et al.* Biotechnological uses of RNAi in plants: risk assessment considerations. *Trends in Biotechnology* **33**, 145-147, doi:https://doi.org/10.1016/j.tibtech.2014.12.003 (2015).
3. Mansoor, S., Amin, I., Hussain, M., Zafar, Y. & Briddon, R. W. Engineering novel traits in plants through RNA interference. *Trends in plant science* **11**, 559-565 (2006).
4. Fujii, N., Inui, T., Iwasa, K., Morishige, T. & Sato, F. Knockdown of berberine bridge enzyme by RNAi accumulates (S)-reticuline and activates a silent pathway in cultured California poppy cells. *Transgenic research* **16**, 363-375 (2007).
5. Sukenik, S. C. *et al.* Transient Recombinant Protein Production in Glycoengineered Nicotiana benthamiana Cell Suspension Culture. *International journal of molecular sciences* **19**, 1205 (2018).
6. Small, I. RNAi for revealing and engineering plant gene functions. *Current Opinion in Biotechnology* **18**, 148-153, doi:https://doi.org/10.1016/j.copbio.2007.01.012 (2007).
7. Williamson, V. M. & Kumar, A. Nematode resistance in plants: the battle underground. *Trends in Genetics* **22**, 396-403, doi:https://doi.org/10.1016/j.tig.2006.05.003 (2006).
8. Huang, G., Allen, R., Davis, E. L., Baum, T. J. & Hussey, R. S. Engineering broad root-knot resistance in transgenic plants by RNAi silencing of a conserved and essential root-knot nematode parasitism gene. *Proceedings of the National Academy of Sciences* **103**, 14302-14306 (2006).
9. Schwab, F. *et al.* Barriers, pathways and processes for uptake, translocation and accumulation of nanomaterials in plants–Critical review. *Nanotoxicology* **10**, 257-278 (2016).
10. Silva, A. T., Nguyen, A., Ye, C., Verchot, J. & Moon, J. H. Conjugated polymer nanoparticles for effective siRNA delivery to tobacco BY-2 protoplasts. *BMC Plant Biology* **10**, 291, doi:10.1186/1471-2229-10-291 (2010).
11. Burch-Smith, T. M., Anderson, J. C., Martin, G. B. & Dinesh-Kumar, S. P. Applications and advantages of virus-induced gene silencing for gene function studies in plants. *The Plant Journal* **39**, 734-746, doi:10.1111/j.1365-313X.2004.02158.x (2004).
12. Godge, M. R., Purkayastha, A., Dasgupta, I. & Kumar, P. P. RETRACTED ARTICLE: Virus-induced gene silencing for functional analysis of selected genes. *Plant Cell Reports* **27**, 209-219, doi:10.1007/s00299-007-0460-2 (2008).
13. Anand, A. & Jones, T. J. in *Agrobacterium Biology: From Basic Science to Biotechnology* (ed Stanton B. Gelvin) 489-507 (Springer International Publishing, 2018).
14. Baltes, N. J., Gil-Humanes, J. & Voytas, D. F. Genome Engineering and Agriculture: Opportunities and Challenges. *Progress in Molecular Biology and Translational Science* (2017).
15. Song, S., Hao, Y., Yang, X., Patra, P. & Chen, J. Using gold nanoparticles as delivery vehicles for targeted delivery of chemotherapy drug fludarabine phosphate to treat hematological cancers. *Journal of nanoscience and nanotechnology* **16**, 2582-2586 (2016).
16. Mizrachi, A. *et al.* Tumour-specific PI3K inhibition via nanoparticle-targeted delivery in head and neck squamous cell carcinoma. *Nature Communications* **8**, 14292 (2017).
17. Demirer, G. S. & Landry, M. P. Delivering Genes to Plants. *CHEMICAL ENGINEERING PROGRESS* **113**, 40-45 (2017).
18. Chang, F.-P. *et al.* A simple plant gene delivery system using mesoporous silica nanoparticles as carriers. *Journal of Materials Chemistry B* **1**, 5279-5287, doi:10.1039/C3TB20529K (2013).

19. Hussain, H. I., Yi, Z., Rookes, J. E., Kong, L. X. & Cahill, D. M. Mesoporous silica nanoparticles as a biomolecule delivery vehicle in plants. *Journal of Nanoparticle Research* **15**, 1676, doi:10.1007/s11051-013-1676-4 (2013).
20. Martin-Ortigosa, S. *et al.* Parameters Affecting the Efficient Delivery of Mesoporous Silica Nanoparticle Materials and Gold Nanorods into Plant Tissues by the Biolistic Method. *Small* **8**, 413-422, doi:doi:10.1002/smll.201101294 (2012).
21. Demirer, G. S. *et al.* High Aspect Ratio Nanomaterials Enable Delivery of Functional Genetic Material Without DNA Integration in Mature Plants. *bioRxiv*, 179549, doi:10.1101/179549 (2018).
22. Martin-Ortigosa, S. *et al.* Mesoporous silica nanoparticle-mediated intracellular Cre protein delivery for maize genome editing via loxP site excision. *Plant physiology* **164**, 537-547 (2014).
23. Mitter, N. *et al.* Clay nanosheets for topical delivery of RNAi for sustained protection against plant viruses. *Nature Plants* **3**, 16207, doi:10.1038/nplants.2016.207 https://www.nature.com/articles/nplants2016207 - supplementary-information (2017).
24. Wong, M. H. *et al.* Lipid exchange envelope penetration (LEEP) of nanoparticles for plant engineering: A universal localization mechanism. *Nano letters* **16**, 1161-1172 (2016).
25. Giraldo, J. P. *et al.* Plant nanobionics approach to augment photosynthesis and biochemical sensing. *Nature materials* **13**, 400-408 (2014).
26. Wu, Y., Phillips, J. A., Liu, H., Yang, R. & Tan, W. Carbon nanotubes protect DNA strands during cellular delivery. *ACS nano* **2**, 2023-2028 (2008).
27. Zheng, M. *et al.* DNA-assisted dispersion and separation of carbon nanotubes. *Nature materials* **2**, 338 (2003).
28. Wang, H. *et al.* High-yield sorting of small-diameter carbon nanotubes for solar cells and transistors. *ACS nano* **8**, 2609-2617 (2014).
29. Liu, Q. *et al.* Carbon nanotubes as molecular transporters for walled plant cells. *Nano letters* **9**, 1007-1010 (2009).
30. Serag, M. F. *et al.* Trafficking and subcellular localization of multiwalled carbon nanotubes in plant cells. *ACS nano* **5**, 493-499 (2010).
31. Wong, M. H. *et al.* Nitroaromatic detection and infrared communication from wild-type plants using plant nanobionics. *Nature materials* **16**, 264-272 (2017).
32. Williams, R. M. *et al.* Noninvasive ovarian cancer biomarker detection via an optical nanosensor implant. *Science Advances* **4**, eaaq1090, doi:10.1126/sciadv.aaq1090 (2018).
33. Wang, P., Lombi, E., Zhao, F. J. & Kopittke, P. M. Nanotechnology: A New Opportunity in Plant Sciences. *Trends Plant Sci* **21**, 699-712, doi:10.1016/j.tplants.2016.04.005 (2016).
34. Nair, R. *et al.* Nanoparticulate material delivery to plants. *Plant Science* **179**, 154-163, doi:https://doi.org/10.1016/j.plantsci.2010.04.012 (2010).
35. Khodakovskaya, M. *et al.* Carbon nanotubes are able to penetrate plant seed coat and dramatically affect seed germination and plant growth. *ACS nano* **3**, 3221-3227 (2009).
36. Kalantidis, K., Tsagris, M. & Tabler, M. Spontaneous short-range silencing of a GFP transgene in Nicotiana benthamiana is possibly mediated by small quantities of siRNA that do not trigger systemic silencing. *The Plant Journal* **45**, 1006-1016, doi:doi:10.1111/j.1365-313X.2006.02664.x (2006).
37. Tang, W. *et al.* Post-transcriptional gene silencing induced by short interfering RNAs in cultured transgenic plant cells. *Genomics, proteomics & bioinformatics* **2**, 97-108 (2004).
38. Agaësse, G., Barbollat-Boutrand, L., El Kharbili, M., Berthier-Vergnes, O. & Masse, I. p53 targets TSPAN8 to prevent invasion in melanoma cells. *Oncogenesis* **6**, e309, doi:10.1038/oncsis.2017.11 (2017).
39. Choi, J. H. & Strano, M. S. Solvatochromism in single-walled carbon nanotubes. *Applied Physics Letters* **90**, 223114 (2007).

40. Yoshioka, H. *et al.* Nicotiana benthamiana gp91phox homologs NbrbohA and NbrbohB participate in H2O2 accumulation and resistance to Phytophthora infestans. *The Plant Cell* **15**, 706-718 (2003).
41. Kashyap, P. L., Xiang, X. & Heiden, P. Chitosan nanoparticle based delivery systems for sustainable agriculture. *International Journal of Biological Macromolecules* **77**, 36-51, doi:https://doi.org/10.1016/j.ijbiomac.2015.02.039 (2015).
42. Goodman, C. M., McCusker, C. D., Yilmaz, T. & Rotello, V. M. Toxicity of Gold Nanoparticles Functionalized with Cationic and Anionic Side Chains. *Bioconjugate Chemistry* **15**, 897-900, doi:10.1021/bc049951i (2004).
43. Qi, Y. *et al.* Increasing frequencies of site-specific mutagenesis and gene targeting in Arabidopsis by manipulating DNA repair pathways. *Genome research*, gr. 145557.145112 (2013).
44. Del Bonis-O'Donnell, J. T. *et al.* Engineering Molecular Recognition with Bio-mimetic Polymers on Single Walled Carbon Nanotubes. *JoVE (Journal of Visualized Experiments)*, e55030 (2017).
45. Beyene, A. G., Demirer, G. S. & Landry, M. P. Nanoparticle-Templated Molecular Recognition Platforms for Detection of Biological Analytes. *Current protocols in chemical biology*, 197-223 (2016).
46. Schmittgen, T. D. & Livak, K. J. Analyzing real-time PCR data by the comparative CT method. *Nature protocols* **3**, 1101 (2008).
47. Kruss, S. *et al.* Neurotransmitter detection using corona phase molecular recognition on fluorescent single-walled carbon nanotube sensors. *Journal of the American Chemical Society* **136**, 713-724 (2014).